

Harnessing second-order optical nonlinearities at interfaces in multilayer silicon-oxy-nitride waveguides

Dylan F. Logan, Ali B. Alamin Dow, Dmitri Stepanov, Payam Abolghasem, Nazir P. Kherani et al.

Citation: *Appl. Phys. Lett.* **102**, 061106 (2013); doi: 10.1063/1.4792272

View online: <http://dx.doi.org/10.1063/1.4792272>

View Table of Contents: <http://apl.aip.org/resource/1/APPLAB/v102/i6>

Published by the [American Institute of Physics](http://www.aip.org).

Additional information on *Appl. Phys. Lett.*

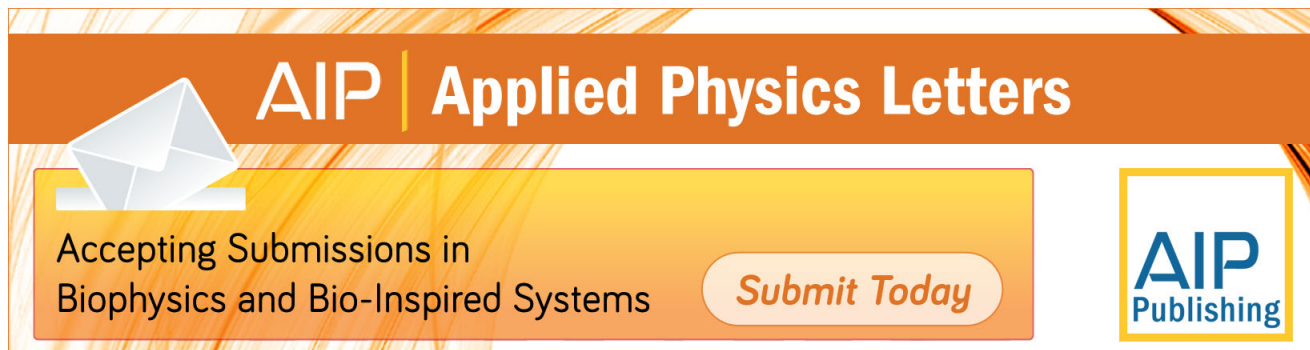
Journal Homepage: <http://apl.aip.org/>

Journal Information: http://apl.aip.org/about/about_the_journal

Top downloads: http://apl.aip.org/features/most_downloaded

Information for Authors: <http://apl.aip.org/authors>

ADVERTISEMENT



AIP | Applied Physics Letters

Accepting Submissions in
Biophysics and Bio-Inspired Systems

Submit Today

AIP
Publishing

Harnessing second-order optical nonlinearities at interfaces in multilayer silicon-oxy-nitride waveguides

Dylan F. Logan,¹ Ali B. Alamin Dow,¹ Dmitri Stepanov,² Payam Abolghasem,¹ Nazir P. Kherani,^{1,2} and Amr S. Helmy^{1,a)}

¹*Department of Electrical and Computer Engineering, University of Toronto, 10 King's College Road, Toronto, Ontario M5S 1A7, Canada*

²*Department of Materials Science and Engineering, University of Toronto, 184 College Street, Toronto, Ontario M5S 3E4, Canada*

(Received 21 December 2012; accepted 31 January 2013; published online 12 February 2013)

We demonstrate multi-layer silicon-oxy-nitride (SiON) waveguides as a platform for broadband tunable phase-matching of second-order nonlinear interactions arising at material interfaces. Second-harmonic generation (SHG) is measured with a 2 ps pulsed pump of 1515–1535 nm wavelength, where 6 nW power is generated by an average pump power of 30 mW in a 0.92 mm long device. The wavelength acceptance bandwidth of the SHG is as broad as 20 nm due to the low material dispersion of SiON waveguides. The waveguide structure provides a viable method for utilizing second order nonlinearity for light generation and manipulation in silicon photonic circuits. © 2013 American Institute of Physics. [<http://dx.doi.org/10.1063/1.4792272>]

Second-order nonlinear effects are traditionally outside the realm of silicon photonics. The bulk second-order nonlinear susceptibility ($\chi^{(2)}$) vanishes in silicon and silicon-based dielectrics due to their inversion symmetry. However, significant progress has been made in exploiting $\chi^{(2)}$ nonlinearities that appear when this symmetry is broken upon application of stress¹ or at interfaces between dissimilar materials.² The prospect of implementing nonlinear wavelength conversion on a silicon platform is an attractive low-cost route towards realizing advanced classical and quantum functionality at the chip-level. The manipulation of $\chi^{(2)}$ within this material system offers a promising alternative to the current effort of utilizing weaker third-order effects, which require cavity or slow-light enhancement, for applications practical in signal processing and quantum optics.^{3,4} Specifically, using silicon-oxy-nitride (SiON) as the optical material has two distinct advantages. First, the large transparency window of SiO₂ and Si₃N₄ between 0.35 and 3 μm ^{5,6} permits nonlinear interactions over a larger spectral range than is possible with semiconductor waveguides. Second, the Kerr nonlinearity is 100 times weaker in comparison to semiconductors,⁷ limiting the shortcomings caused by two-photon absorption and permitting the utilization of higher pump powers.

Second-harmonic generation (SHG) reflected from the surfaces of centro-symmetric materials is a well-established surface characterization technique.⁸ At an interface between two materials, the second-order nonlinearity is expressed by a surface- $\chi^{(2)}$ tensor, for which there are three distinct non-zero elements. The $\chi_{\perp\perp\perp}^{(2)}$ element (where \perp is the interface normal) is the largest tensor element by an order of magnitude for Si₃N₄,⁹ SiO₂,¹⁰ and Si surfaces.¹¹ This is attributed to dangling bonds that form a distribution of surface dipoles, pointing normal to the surface.¹² Consequently, the largest nonlinear interaction will involve the optical field components normal to the interface.¹²

In a planar waveguide structure, surface second-order nonlinearities may arise at the waveguide sidewalls and/or at the interfaces between adjacent materials. Recently, Si₃N₄ ring resonators have been used to provide resonant enhancement for the excitation field and hence the nonlinear interaction.² The pump and SH fields were TE-polarized, indicating that a surface contribution utilizing the $\chi_{\perp\perp\perp}^{(2)}$ element originated from the waveguide sidewalls. The nonlinearities in these cases however pronounced are still limited to a single or a set of interfaces as opposed to a bulk coefficient.

In this letter, we demonstrate a multilayer-core anti-resonant reflecting optical waveguide (ARROW) platform as a travelling wave (non-cavity-enhanced) structure for efficient utilization of the second-order nonlinear effect. The structure is formed of SiON layers of minimal composition variation and exploits the $\chi_{\perp\perp\perp}^{(2)}$ arising from the interfaces between these layers. The nonlinearity is assessed using second-harmonic generation, where both pump and SH modes are TM-polarized. The ARROW serves two functions in this platform as confirmed through the SHG. First, the structure is dispersion-engineered so that the pump mode at $\lambda_p = 1540$ nm and the ARROW SH mode at $\lambda_{SH} = 770$ nm wavelengths are phase matched through modal phase-matching. Second, we have designed the structure such that the electric fields are maximized at interfaces and hence fully exploit the embedded interface nonlinearity.

The multi-layer structure, shown in Fig. 1(a), contains four SiON layers deposited by PECVD on a SiO₂-on-Si substrate. The thickness of the SiO₂ layer was 5 μm . The SiON layer composition was varied during growth by adjusting the SiH₄/N₂O flow rate, providing the index contrast shown in Fig. 1(c).¹³ The ARROW structure serves to confine the second-harmonic mode with a large field concentrated within the low index core region. The pump mode, on the other hand, is confined by the aggregate structure in a conventional total internal reflection (TIR) fundamental mode. The layer thicknesses were calculated so that the two interacting modes were phase-matched. This was used to obtain an optimum

^{a)} Author to whom correspondence should be addressed. Electronic mail: a.helmy@utoronto.ca.

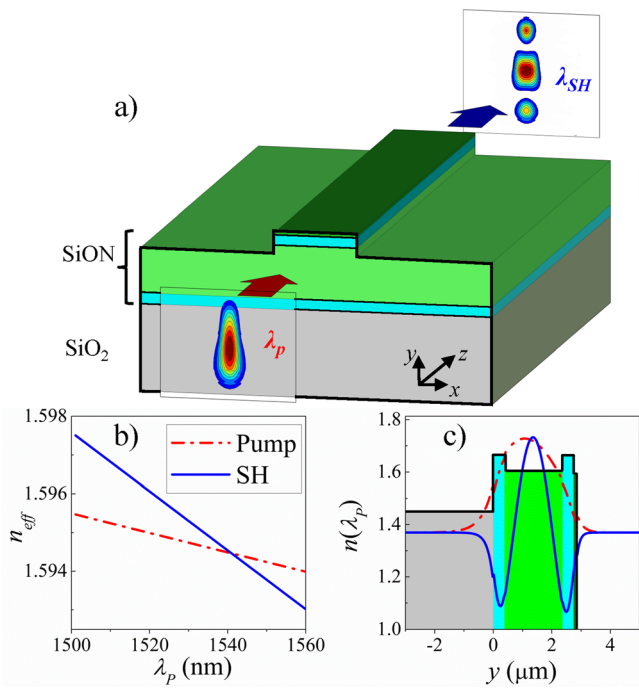


FIG. 1. (a) Schematic of the designed SiON ARROW structure, with the optical field of the phase-matched pump and SH modes illustrated; (b) the effective index n_{eff} of the pump (red) and SH (blue) mode, plotted as a function of pump wavelength λ_p ; (c) refractive index (n) variation of ARROW mode, with pump (red) and SH (blue) field profiles (E_y) overlaid.

structure with maximal nonlinear conversion efficiency given the number of layers and the minimal refractive index difference between the SiON layers. Ridge waveguides were patterned and etched to provide lateral optical confinement. The waveguide width and etch depth were chosen to be 3.1 and 1.3 μm , respectively, such that the waveguide would only support a single mode at λ_p .

The nonlinear interaction is characterized by two parameters: the spatial overlap factor ζ [1/m] and the effective second-order nonlinear coefficient d_{eff} [m/V].¹⁴ The calculation of ζ is identical to that of other waveguide systems. The value of d_{eff} , however, is in this case the sum over the N interfaces of the product of the optical fields and the susceptibility tensor element⁸

$$d_{eff} = \frac{\sum_{i=0}^N \chi_{yyy}^{(2)}(i) \int [E_y(x, y_i, \omega)]^2 E_y(x, y_i, 2\omega) dx}{\int [E_y(x, y, \omega)]^2 E_y(x, y, 2\omega) dx dy}, \quad (1)$$

where i is a layer index, $\chi_{yyy}^{(2)}(i)$ is the susceptibility tensor element at the interface between layer i and $i+1$ (at location y_i), and E_y is the component of the local field. Assuming that the value of $\chi_{yyy}^{(2)}$ is minimally variant between layers, it can be moved outside of the summation and it is possible to optimize the structure by maximizing the remaining factor. This predicts that the optimum device is one in which both interacting modes contain large optical fields at each interface. The optimized phase-matched structure is specified in Fig. 1 and has a simulated $\zeta = 1.45 \times 10^5 \text{ m}^{-1}$ and $d_{eff} = 1.41 \times 10^6 \text{ m}^{-1} \times \chi_{yyy}^{(2)}$. The effective index of both modes is

plotted in Fig. 1(b), indicating a phase-matching wavelength of 1540 nm.

The waveguides were characterized in an end-fire coupling set-up with free-space optical input and output. The pump source was a Ti:sapphire pumped optical parametric oscillator (OPO) with a repetition rate of 76 MHz and 2 ps pulse width. The pump was coupled into the waveguide using a Newport M-60 \times /0.85 NA objective lens. The transmitted light was collected using a Newport M-40 \times /0.65 NA objective lens. The output light was spectrally filtered with a 1.1 μm long-wavelength pass filter; the reflected light was detected using a silicon power meter and the transmitted light detected using a germanium power meter. Reference curves taken without any sample present indicate no SHG artifact in the system that is measurable above the noise floor of the silicon power meter.

The average transmitted pump power (at 1530 nm, TM-polarized) for each waveguide length is plotted as red squares in Fig. 2, from which the propagation loss and coupling loss are extracted using the cut-back method to be $\alpha_p = 2.48 \pm 2.18 \text{ dB/cm}$ and $4.7 \pm 0.3 \text{ dB/facet}$, respectively. Similarly, the 770 nm Ti:sapphire laser was directly coupled into the waveguide, and the measured transmission is plotted as blue circles. From this, the propagation loss for the TM-polarized second-harmonic mode is estimated to be $\alpha_{SH} = 16.66 \pm 0.92 \text{ dB/cm}$. The propagation loss of the pump is larger than previously reported for SiON waveguides,¹⁵ presumably due to scattering from the waveguide sidewalls. The propagation loss at the second-harmonic wavelength is significantly larger, further evidence that the propagation loss is dominated by a scattering process. Moreover, the confinement of the ARROW mode is poor due to the modest etch depth, and therefore, suffers from leakage loss.

The average power of the pulsed pump was fixed at the chip input with a value of $P_p = 30 \text{ mW}$, while the wavelength was varied and the transmitted power reaching the silicon photodiode P_{SH} monitored. Examples of the tuning curves resulting from these scans are shown in Fig. 3(a). The peak in P_{SH} indicates an enhancement in SHG efficiency, provided by phase-matching between the pump and second-harmonic modes. The phase-matching wavelength varies between devices (regardless of length), by approximately 20 nm, due its dependence on the variations in layer thickness and ridge width across the wafer. For instance, the derivatives of phase-matching wavelength with respect to

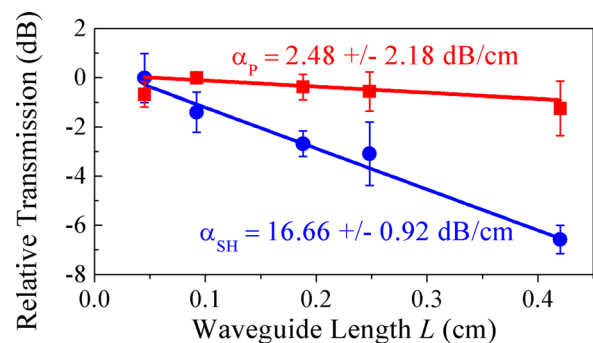


FIG. 2. Relative waveguide transmission at 1530 nm (red squares) and 770 nm (blue circles) as a function of length L , yielding estimates of propagation losses α_p and α_{SH} .

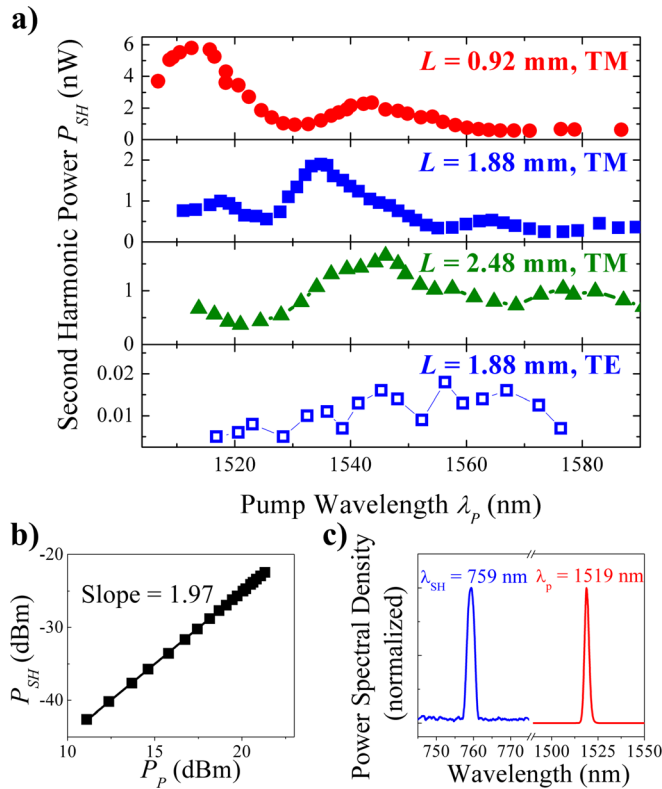


FIG. 3. (a) Sample tuning curves for varying chip length and input polarization; (b) silicon photodiode power plotted against on-chip pump power, and (c) spectrum of pump and SHG for $L = 0.92$ mm and $\lambda_p = 1519$ nm.

core thickness and etch depth are simulated to be 0.32 and 0.26 nm/nm, while the fabrication tolerance/control of these values is as large as 50 nm.

The observed wavelength acceptance bandwidth of the SHG is relatively broad (15–20 nm). However, this is not attributed to the waveguide losses, as semiconductor waveguides with similar propagation loss produce much sharper phase-matched peaks of <2 nm bandwidth.¹⁶ The broadband SHG tuning curve is attributed to the low material dispersion of the waveguides (indicated in Fig. 1(b)) that is characteristic of dielectric structures operated at wavelengths far from the band edge.

A similar tuning curve was produced for TE-polarized pump, for the $L = 1.88 \pm 0.04$ mm long device, and yielded no measurable signal on the silicon photodiode, indicating that second-harmonic generation with a TE-polarized pump is not detectable in this structure. The second-harmonic signal was confirmed to be TM-polarized for all peaks, so the interaction was categorized as a type-0 process where both pump and SH are TM polarized. There is no mechanism for this interaction that originates from the waveguide sidewall, since its surface $\chi_{yyy}^{(2)} = \chi_{zzz}^{(2)} = 0$ pm²/V in the coordinate system of Fig. 1.¹² Also, the field at the top surface of the waveguide is very weak (see Fig. 1(c)), ruling it out as the dominant source of the nonlinearity. Consequently, we can conclude that the interface $\chi^{(2)}$ arises from interfaces within the multi-layer structure.

The relationship between P_p and P_{SH} for $L = 0.92$ mm is plotted in Fig. 3(b). As indicated by the slope of the log-log plot, the behaviour is quadratic as expected for second-harmonic generation. There is no evidence of P_{SH} saturation

at high P_p caused by the onset of two-photon absorption, due to the low value of $\chi^{(3)}$ in this material system. A sample spectrum measured at the output is shown in Fig. 3(c), where the 1519 nm pump produces a second-harmonic peak at 759 nm.

The peak external efficiency of the $L = 0.92 \pm 0.04$ mm device is $5.94 \pm 0.98 \times 10^{-4}$ %/W, and can be normalized to $7.02 \pm 1.15 \times 10^{-2}$ % W⁻¹ cm⁻². This calculation does not take into account the out-coupling loss of the ARROW mode, the transmission through the collection objective lens (estimated to be 78%), and the reflection loss at the 1.1 μ m long-wavelength pass filter. Consequently, the above number underestimates the peak internal efficiency. Given the low influence of two-photon absorption, we can also extract an equivalent CW efficiency by evaluating with respect to the peak powers (rather than average power), which yields a value of $\eta = 5.7 \pm 0.4 \times 10^{-7}$ %/W.

The theoretical variation in conversion efficiency η with length L , when the phase-matching condition is satisfied, is¹⁴

$$\eta = \frac{8\pi^2}{n_{eff}^3 \epsilon_0 c \lambda_p^2} [d_{eff} \xi]^2 L^2 \times \exp\left[-\left(\alpha_p + \frac{\alpha_{SH}}{2}\right)L\right] \frac{\sinh^2\left[\left(\alpha_p - \frac{\alpha_{SH}}{2}\right)\frac{L}{2}\right]}{\left[\left(\alpha_p - \frac{\alpha_{SH}}{2}\right)\frac{L}{2}\right]^2}, \quad (2)$$

where n_{eff} is the mode index, ϵ_0 is the permittivity of free-space, c is the speed of light in vacuum, and the other parameters have been defined above. This indicates that the quadratic dependence of P_{SH} on length L becomes degraded for cases associated with significant propagation loss. The efficiencies extracted from the peaks of the tuning curves are plotted in Fig. 4. Also plotted as a solid line is a fit of Eq. (2), using the values of α_p and α_{SH} obtained from Fig. 2, for which a value of the product $d_{eff} \times \xi = 1.83 \pm 0.93 \times 10^{-9}$ V⁻¹ is extracted. Given the simulated value of $\xi = 1.45 \times 10^5$ m⁻¹ for the designed structure, we approximate the effective nonlinearity of this structure to be $d_{eff} = 1.3 \pm 0.7 \times 10^{-14}$ m/V. This nonlinearity is similar in magnitude to that estimated for other SiN waveguide structures.² Further, by using the modeled value of $d_{eff} = 1.41 \times 10^6$ m⁻¹ $\times \chi_{yyy}^{(2)}$, we estimate the value of the surface nonlinearity tensor element to be $\chi_{yyy}^{(2)} = 9.0 \pm 4.6 \times 10^{-21}$ m²/V. This is similar to the value reported (for 1 μ m wavelength) for SiO₂ surfaces (6 – 9×10^{-21} m²/V)¹⁰ and less than that for silicon surfaces (for 745 nm wavelength) (6×10^{-18} m²/V).¹¹

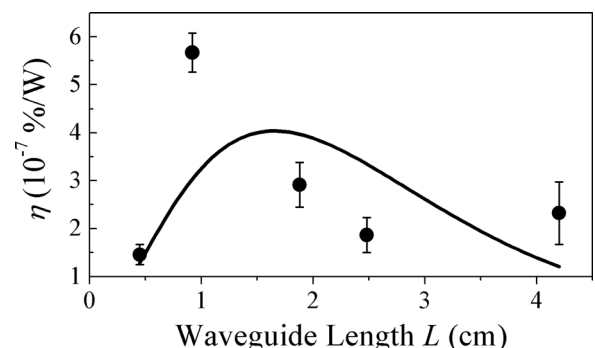


FIG. 4. Measured efficiency versus device length (points) and fit of Eq. (2) (line).

The general agreement of the data points with the theoretical prediction in Fig. 4 indicates that large propagation losses do indeed limit the peak efficiency. Since the source of the nonlinearity is embedded in the device, the efficiency can be improved by increasing the number of interfaces within the core, as indicated in Eq. (1). The nonlinear interaction was not enhanced by cavity or slow light effects, although such structures can be also employed to further strengthen the efficiency, as is commonly done for third-order nonlinear interactions.^{3,4}

The introduction of local inhomogeneous strain at the interfaces, due to compositional differences between layers, is expected to further improve d_{eff} .¹⁷ However, the inhomogeneous bulk strain levels reported in silicon waveguides¹ are probably not present in these devices. The SiON layers are oxygen-rich and are similar in density to the SiO₂ substrate on which they are grown. The SiON growth processes use an N₂O/SiH₄ ratio ranging from 10.6 to 12.9 (with no NH₃), power ranging from 20 to 60 W and pressure fixed at 950 mTorr.¹³ The compressive stress in a single SiON layer is estimated to be 50–150 MPa,^{18–20} but varies between layers of differing composition by only approximately 10 MPa.^{18,19} The strain is therefore homogeneous throughout the multi-layer structure, and does not feature large gradients needed to produce a significant contribution to the nonlinearity.^{1,17}

While the d_{eff} is lower than that obtained in strained silicon waveguides ($>10^{-11}$ m/V),¹ the larger bandgap energy of SiON provides it with distinct advantages over silicon structures. First, this platform permits wavelength conversion over a larger transparency window that extends to visible wavelengths. Second, third-order nonlinear effects such as two-photon absorption are far less limiting at C-band wavelengths (for which the photon energy is less than half of the bandgap energy). Last, due to its low material dispersion at wavelengths in the C-band, it produces very broadband phase-matched wavelength conversion.

In summary, we have utilized SiON layers of similar composition and minimal local strain for harnessing second-order interface nonlinearities. The layer configuration is designed

to support an ARROW mode in order to phase-match weak nonlinear processes originating at five interfaces within the core.

This work was supported by the Ontario Research Fund-Research Excellence program, the Mitacs Elevate postdoctoral fellowship, Natural Sciences and Engineering Research Council of Canada, and the University of Toronto.

¹M. Cazzanelli, F. Bianco, E. Borga, G. Pucker, M. Ghulinyan, E. Degoli, E. Luppi, V. Vénier, S. Ossincini, D. Modotto, S. Wabnitz, R. Pierobon, and L. Pavesi, *Nature Mater.* **11**, 148 (2011).

²J. S. Levy, M. A. Foster, A. L. Gaeta, and M. Lipson, *Opt. Express* **19**, 11415 (2011).

³M. A. Foster, J. S. Levy, O. Kuzucu, K. Saha, M. Lipson, and A. L. Gaeta, *Opt. Express* **19**, 14233 (2011).

⁴J. Li, L. O' Faolain, and T. Krauss, *Opt. Express* **20**, 17474 (2012).

⁵S. V. Deshpande, E. Gulari, S. W. Brown, and S. C. Rand, *J. Appl. Phys.* **77**, 6534 (1995).

⁶R. Kitamura, L. Pilon, and M. Jonasz, *Appl. Opt.* **46**, 8118 (2007).

⁷M.-C. Tien, J. F. Bauters, M. J. R. Heck, D. J. Blumenthal, and J. E. Bowers, *Opt. Express* **18**, 23562 (2010).

⁸Y. R. Shen, *Nature* **337**, 519 (1989).

⁹T. Ning, H. Pietarinen, O. Hyvärinen, J. Simonen, G. Genty, and M. Kauranen, *Appl. Phys. Lett.* **100**, 161902 (2012).

¹⁰F. J. Rodriguez, F. X. Wang, and M. Kauranen, *Opt. Express* **16**, 8704 (2008).

¹¹Y. Q. An, R. Carriès, and M. C. Downer, *Phys. Rev. B.* **75**, 241307(R) (2007).

¹²S. Lettieri, S. Di Finizio, P. Maddalena, V. Ballarini, and F. Giorgis, *Appl. Phys. Lett.* **81**, 4706 (2002).

¹³A. B. Alamin Dow, K. Leong, A. B. Gougam, H. Alizadeh, and N. P. Kherani, *Proc. SPIE* **8069**, 80690S (2011).

¹⁴R. L. Sutherland, *Handbook of Nonlinear Optics* (Marcel Dekker, Inc., New York, USA, 1996).

¹⁵L. Leick, K. Zenth, C. Laurent-Lund, T. Koster, L.-U. A. Andersen, L. Wang, B. H. Larsen, L. P. Nielsen, and K. E. Mattsson, in OFC 2004, February 2004, paper MF40.

¹⁶P. Abolghasem, J. Han, B. J. Bijlani, A. Arjmand, and A. S. Helmy, *IEEE Photon. Technol. Lett.* **21**, 1462 (2009).

¹⁷C. Schriever, C. Bohley, and R. B. Wehrspohn, *Opt. Lett.* **35**, 273 (2010).

¹⁸K. D. Mackenzie, D. J. Johnson, M. W. DeVre, R. J. Westerman, and B. H. Reelfs, in *Proceedings of the Symposium on Silicon Nitride and Silicon Dioxide Thin Insulating Films and Other Emerging Dielectrics VIII* (2005), pp. 148–159, Paper No. PV2005-01.

¹⁹T. Storgaard-Larsen and O. Leistiko, *J. Electrochem. Soc.* **144**, 1505 (1997).

²⁰D. R. Harding, L. U. T. Ogbuji, and M. J. Freeman, *J. Appl. Phys.* **78**, 1673 (1995).